Crystal chemistry and intracrystalline relationships of orthopyroxene in a suite of high pressure ultramafic nodules from the 'Newer Volcanics' of Victoria, Australia

GIANMARIO MOLIN AND MARILENA STIMPFL

Dipartimento di Mineralogia e Petrologia, Universita' di Padova, Corso Garibaldi 37, 35100 Padova, Italy

Abstract

A suite of orthopyroxenes from spinel lherzolite xenoliths associated with basanites occurring in the Victorian (Australia) post-Pliocene 'Newer Volcanics' province was investigated by means of a crystal chemical methodology which provides accurate site occupancy and site configuration parameters.

The *M*1 configuration is essentially constrained by Al^{VI} rather than Fe^{2+}. In addition, Fe^{3+}, Cr^{3+} and Ti^{4+} are confined to *M*1 (Molin, 1989) and Al^{IV} to *TB*. *M*2 is controlled by $Fe^{2+}_{M2} \rightleftharpoons Mg_{M2}$, constrained by $(Fe^{2+} + Ca)_{M2} > 0.14$ atoms per formula unit (p.f.u.). Cation substitution in *TB* and *M*2 constrains the sum of the volumes of the respective polyhedra $V_{TB} + V_{M2}$ to remain essentially constant. Therefore, *M*2 favours the retention of the large Fe^{2+} up to melting-point, causing non-ideality of this iron-depleted orthopyroxene. As a consequence, the investigated orthopyroxene can be considered an ultimate Fe^{2+} carrier during partial mantle melting.

KEYWORDS: orthopyroxene, crystal chemistry, spinel lherzolite.

Introduction

A CRYSTAL chemical study based on single crystal X-ray diffraction techniques combined with microanalysis of the same crystal was carried out on a suite of orthopyroxenes from high-pressure lherzolite xenoliths associated with basanite at Mt Leura and Mt Porndon, in the Victorian (Australia) 'Newer Volcanics' (Irving, 1974; Frey and Green, 1974; Ellis, 1976; O'Reilly *et al.*, 1989). A similar study on the coexisting clinopyroxene had demonstrated that intracrystalline relationships are dominated by cations smaller than Mg^{2+} in ionic radius, particularly Al^{3+}, which is strongly depleted with increasing the Mg/(Mg+Fe^{2+}) ratio (mg) (Dal Negro *et al.*, 1984). The Fe^{2+}_{M2} is more stably retained than Fe^{2+}_{M1} in clinopyroxene from more refractory harzburgitic assemblages. This implies that Fe^{2+} partitioning to mantle-derived melts is a function of the degree of melting.

The Mg–Fe^{2+} ordering in *M*1-*M*2 respectively is pressure-dependent as well as mg-dependent (Cundari *et al.*, 1986). Consequently, knowledge of intracrystalline relationships is essential in constraining hypotheses of melting processes as well as applications of order-disorder relationships to geothermometers.

The extent of Mg–Fe^{2+} ordering in *M*1-*M*2 respectively, as a function of temperature and bulk composition, was undertaken (Molin, 1989) on two orthopyroxene crystals of xenoliths from Mt. Leura, samples LE4 and LE10, characterized by similar Mg/Fe^{2+} ratios and different contents in trivalent ions R^{3+}, (R^{3+} = Al^{VI} + Cr^{3+} + Ti^{4+} + Fe^{3+}). Disordering was more easily achieved when the R^{3+} content was low; up to the highest temperatures (1050–1150°C) R^{3+} restricted to *M*1.

The aim of this study was to investigate the intracrystalline behaviour of the orthopyroxene in the xenoliths, compared to that of the coexisting clinopyroxene. Petrographic descriptions of the specimen material is given in Dal Negro *et al.* (1984) and represents the modal variation reported for Mt. Leura (LE) and Mt. Porndon (PD) lherzolitic xenoliths.

Mineralogical Magazine, June 1994, Vol. 58, pp. 325–332

It will be demonstrated that, as in the coexisting clinopyroxene, the most significant variations relate to the configuration of *M*1, but most of the Fe^{2+} is locked in *M*2 at the highest subsolidus temperatures.

Experimental

All the analysed orthopyroxenes were selected under a petrographic microscope from rock sections about 100 μm thick. Only optically homogeneous crystal fragments, usually from the crystal core, were hand-picked. The degree of intra- and intercrystalline homogeneity in crystals from the same nodule was investigated by several point analyses and by the structural refinement of two crystals from LE12, one completely surrounded by olivine (LE12i) and one in contact with clinopyroxene (LE12c).

Structural X-ray refinements and electron microprobe analyses were carried out on the same crystal fragment. Experimental conditions were described in detail by Molin, (1989).

The cation distribution among sites (Table 1) was obtained by the minimization of the squares of the following constraints: (1) balance between atomic fractions and site electron densities for both *M*2 and *M*1 sites; (2) complete site occupancy of *T*, *M*2 and *M*1 sites; (3) bulk valence balance; and (4) charge balance between Al^{IV} and octahedral R^{3+} trivalent ions. The ions Ca^{2+} and Mn^{2+} were assigned to *M*2 and Al^{VI}, Fe^{3+}, Ti^{4+} and Cr^{3+} to *M*1. Calculations were performed by means of MINUIT (James and Ross, 1975). The Fe^{2+} and Mg atomic fractions were independent variables with completely random initial values in the range 0–1 for *M*1 and *M*2 sites.

TABLE 1 Chemical composition and site occupancy of orthopyroxenes based on *M*1 *M*2 T_2 O_6.

	LE4	LE8	LE9	LE10	LE11	LE12i	LE12c	LE20	PD2	PD5	PD6
SiO_2	54.7	57.4	57.1	56.8	56.7	57.2	57.1	55.2	56.4	56.6	55.2
TiO_2	0.13	0.00	0.00	0.00	0.00	0.00	0.00	0.00	0.15	0.05	0.00
Al_2O_3	4.0	0.9	0.4	1.2	2.2	0.9	0.8	3.8	3.2	1.6	4.1
FeO	6.8	5.2	5.8	5.4	5.5	5.4	5.6	6.7	5.5	5.1	6.8
MnO	0.24	0.00	0.00	0.14	0.19	0.16	0.21	0.12	0.20	0.15	0.10
MgO	33.1	35.3	35.1	35.4	34.3	35.2	34.9	33.0	33.8	35.1	33.0
CaO	0.80	0.68	0.31	0.45	0.80	0.64	0.64	0.74	0.80	0.75	0.79
Cr_2O_3	0.26	0.41	0.46	0.48	0.51	0.62	0.72	0.34	0.47	0.66	0.32
Total	100.03	99.89	99.17	99.87	100.20	100.12	99.97	99.90	100.52	99.35	100.31
T site											
Si	1.891	1.968	1.985	1.955	1.942	1.962	1.970	1.906	1.927	1.943	1.901
Al^{IV}	0.109	0.032	0.015	0.045	0.058	0.038	0.030	0.094	0.073	0.057	0.099
	2.000	2.000	2.000	2.000	2.000	2.000	2.000	2.000	2.000	2.000	2.000
*M*1 site											
Mg	0.892	0.957	0.965	0.956	0.929	0.953	0.949	0.891	0.901	0.944	0.886
Fe^{2+}	0.000	0.011	0.021	0.000	0.013	0.009	0.020	0.015	0.027	0.000	0.014
Fe^{3+}	0.044	0.016	0.002	0.026	0.015	0.021	0.012	0.026	0.000	0.028	0.025
Cr	0.007	0.011	0.012	0.013	0.014	0.017	0.019	0.009	0.013	0.018	0.009
Ti	0.003	0.000	0.000	0.000	0.000	0.000	0.000	0.000	0.004	0.001	0.000
Al^{VI}	0.054	0.005	0.000	0.005	0.029	0.000	0.000	0.059	0.055	0.009	0.066
	1.000	1.000	1.000	1.000	1.000	1.000	1.000	1.000	1.000	1.000	1.000
*M*2 site											
Mg	0.813	0.856	0.845	0.852	0.835	0.848	0.842	0.818	0.833	0.852	0.810
Fe^{2+}	0.151	0.119	0.144	0.128	0.131	0.124	0.129	0.152	0.132	0.117	0.158
Ca	0.029	0.025	0.011	0.016	0.029	0.023	0.023	0.027	0.029	0.027	0.029
Mn	0.007	0.000	0.000	0.004	0.005	0.005	0.006	0.003	0.006	0.004	0.003
	1.000	1.000	1.000	1.000	1.000	1.000	1.000	1.000	1.000	1.000	1.000
mg	0.918	0.931	0.916	0.934	0.924	0.931	0.923	0.910	0.916	0.939	0.908
$K_D^{(M1-M2)}$	0.00	0.08	0.13	0.00	0.09	0.60	0.14	0.09	0.19	0.00	0.08

TABLE 2. Polyhedral geometry of orthopyroxene (σ in brackets).

	LE4	LE8	LE9	LE10	LE11	LE12i	LE12c	LE20	PD2	PD5	PD6
a (Å)	18.254(2)	18.258(2)	18.260(2)	18.263(3)	18.261(2)	18.257(2)	18.260(2)	18.253(2)	18.256(3)	18.258(2)	18.245(2)
b (Å)	8.811(1)	8.832(1)	8.835(1)	8.837(1)	8.826(1)	8.829(1)	8.831(1)	8.814(1)	8.819(1)	8.823(1)	8.813(1)
c (Å)	5.200(1)	5.195(1)	5.195(1)	5.196(1)	5.197(1)	5.195(1)	5.195(1)	5.198(1)	5.198(1)	5.193(1)	5.199(1)
V (Å^3)	836.37	837.78	838.00	838.58	837.58	837.48	837.83	836.19	836.99	836.58	835.88
No. obs. refl.	1094	1152	1019	1044	1164	1077	1070	1009	962	1049	1052
R obs.%	2.3	2.2	2.6	2.4	3.4	2.3	2.2	2.6	2.9	3.1	2.3
M1–O1A	2.023(2)	2.027(2)	2.031(2)	2.030(2)	2.027(3)	2.027(2)	2.029(2)	2.027(2)	2.025(2)	2.027(3)	2.022(2)
M1–O1A′	2.144(2)	2.151(2)	2.150(2)	2.151(2)	2.145(3)	2.148(2)	2.148(2)	2.144(2)	2.145(2)	2.146(3)	2.145(2)
M1–O1B	2.055(2)	2.063(2)	2.067(2)	2.064(2)	2.059(3)	2.061(2)	2.064(2)	2.054(2)	2.060(2)	2.058(3)	2.054(2)
M1–O1B′	2.158(2)	2.166(2)	2.169(2)	2.167(2)	2.159(3)	2.165(2)	2.167(2)	2.161(2)	2.159(2)	2.164(3)	2.154(2)
M1–O2A	2.006(2)	2.011(2)	2.013(2)	2.013(2)	2.011(3)	2.012(2)	2.012(2)	2.011(2)	2.010(2)	2.007(3)	2.008(2)
M1–O2B	2.031(2)	2.044(2)	2.048(2)	2.047(2)	2.039(3)	2.044(2)	2.046(2)	2.033(2)	2.036(2)	2.039(3)	2.032(2)
mean	2.070	2.077	2.079	2.079	2.073	2.076	2.077	2.072	2.072	2.073	2.069
V (Å^3)	11.68	11.81	11.85	11.84	11.75	11.80	11.81	11.72	11.72	11.75	11.67
σ^2_{M1}	26.33	25.99	25.59	25.91	25.53	25.70	25.68	25.86	26.33	26.05	26.27
M2–O1A	2.134(2)	2.121(2)	2.119(2)	2.118(2)	2.129(3)	2.122(2)	2.120(2)	2.132(2)	2.130(2)	2.122(3)	2.136(2)
M2–O1B	2.081(2)	2.076(2)	2.077(2)	2.077(2)	2.081(3)	2.080(2)	2.078(2)	2.080(2)	2.080(2)	2.079(3)	2.082(2)
M2–O2A	2.067(2)	2.051(2)	2.048(2)	2.052(2)	2.059(3)	2.054(2)	2.056(2)	2.065(2)	2.059(2)	2.051(3)	2.062(2)
M2–O2B	1.999(2)	1.997(2)	1.994(2)	1.998(2)	1.999(3)	1.997(2)	1.998(2)	1.999(2)	2.001(2)	1.996(3)	2.000(2)
M2–O3A	2.304(2)	2.305(2)	2.303(2)	2.304(2)	2.306(3)	2.305(2)	2.305(2)	2.304(2)	2.304(2)	2.301(3)	2.305(2)
M2–O3B	2.395(2)	2.437(2)	2.448(2)	2.431(2)	2.421(3)	2.433(2)	2.431(2)	2.403(2)	2.410(2)	2.428(3)	2.399(2)
mean	2.163	2.164	2.165	2.163	2.166	2.165	2.165	2.164	2.164	2.163	2.164
V (Å^3)	12.59	12.63	12.64	12.63	12.64	12.63	12.63	12.61	12.61	12.59	12.60
σ^2_{M2}	156.74	152.54	151.54	149.80	155.88	153.74	153.12	155.70	155.80	154.50	156.89
TA–O1A	1.617(1)	1.613(1)	1.612(2)	1.614(2)	1.614(2)	1.613(2)	1.614(2)	1.616(2)	1.616(2)	1.614(3)	1.614(2)
TA–O2A	1.594(2)	1.594(1)	1.590(2)	1.593(2)	1.595(3)	1.592(2)	1.593(2)	1.590(2)	1.594(2)	1.597(3)	1.594(2)
TA–O3A	1.647(2)	1.648(2)	1.649(2)	1.647(2)	1.647(3)	1.647(2)	1.647(2)	1.647(2)	1.650(2)	1.651(3)	1.647(2)
TA–O3A′	1.662(2)	1.660(2)	1.660(2)	1.665(2)	1.664(3)	1.663(2)	1.661(2)	1.661(2)	1.658(2)	1.658(3)	1.662(2)
mean	1.630	1.628	1.628	1.630	1.630	1.629	1.628	1.628	1.629	1.630	1.629
V (Å^3)	2.193	2.187	2.184	2.192	2.193	2.189	2.189	2.187	2.191	2.192	2.190
σ^2_{TA}	36.80	37.49	38.51	37.60	37.35	37.64	37.16	36.89	37.12	39.14	37.18
O3A–O3A–O3A°	160.76	160.40	160.24	160.24	160.76	160.63	160.48	160.60	160.82	160.34	160.98
TB–O1B	1.634(1)	1.625(1)	1.620(2)	1.625(2)	1.628(3)	1.623(2)	1.625(2)	1.630(2)	1.632(2)	1.627(3)	1.633(2)
TB–O2B	1.601(2)	1.595(1)	1.593(2)	1.594(2)	1.601(3)	1.596(2)	1.594(2)	1.602(2)	1.600(2)	1.598(3)	1.602(2)
TB–O3B	1.679(2)	1.674(2)	1.672(2)	1.678(2)	1.677(3)	1.676(2)	1.674(2)	1.676(2)	1.682(2)	1.670(3)	1.676(2)
TB–O3B′	1.686(2)	1.682(2)	1.681(2)	1.682(2)	1.684(3)	1.682(2)	1.683(2)	1.683(2)	1.678(2)	1.684(3)	1.685(2)
mean	1.650	1.644	1.642	1.645	1.647	1.644	1.644	1.648	1.648	1.645	1.649
V (Å^3)	2.290	2.265	2.255	2.268	2.278	2.265	2.266	2.281	2.280	2.267	2.285
σ^2_{TB}	19.57	19.48	19.75	19.22	19.09	19.56	18.91	19.48	19.64	20.17	19.62
O3B–O3B–O3B°	139.11	139.67	139.79	139.38	139.68	139.82	139.54	139.36	139.41	139.63	139.30

σ^2_{M1}, σ^2_{M2} defined by $\sum_{i=1}^{12}(\theta_i-90°)^2/11$; σ^2_{TA}, σ^2_{TB} defined by $\sum_{i=1}^{6}(\theta_i-109.47°)^2/5$ (Robinson *et al.*, 1971)

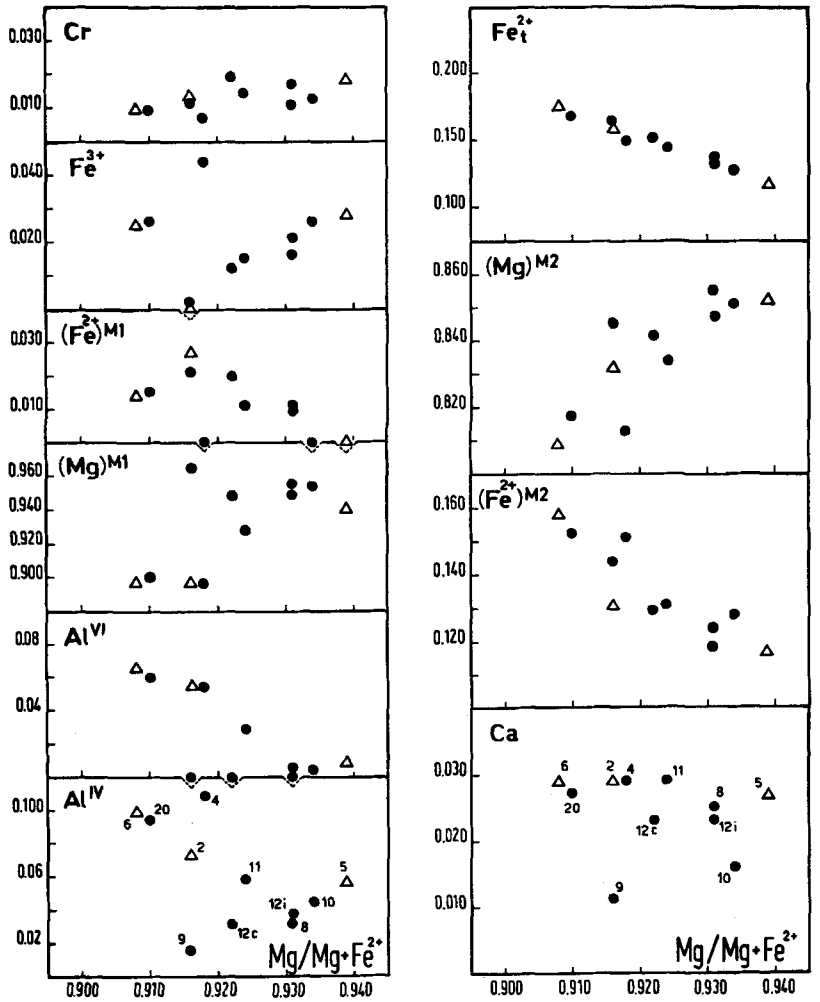

FIG. 1. Compositional variations of orthopyroxene in terms of cations in structural formula *vs.* Mg/(Mg+Fe^{2+}). Filled circles: Mt. Leura samples (LE); open triangles: Mt. Porndon samples (PD).

Crystal-chemistry

Crystal structure parameters, site occupancies and chemical composition of the selected orthopyroxenes are given in Tables 1 and 2.

The selected orthopyroxenes are characterized by a moderate compositional variation, Mg ranging from 1.70 to 1.82 atoms p.f.u. and by a relatively large variation in R^{3+} (R^{3+} = 0.014–0.108 atoms p.f.u.) with dominant Al^{VI} (0.00–0.066 atoms p.f.u.). The Fe^{2+} content (0.117–0.172 atoms p.f.u.) is highly ordered in the *M*2 site (Table 1). Figure 1 illustrates the variations of site occupancies with mg.

The *M*1 polyhedron is a nearly regular octahedron largely filled by Mg^{2+} (0.89–0.98 atoms p.f.u.), Fe^{2+} being particularly low (0.02–0.00 atoms p.f.u.). Its volume variation is mainly controlled by Al^{VI}, whose ionic radius (I.R. = 0.56 Å) is smaller than that of Mg^{2+} (I.R. = 0.72 Å) (Shannon, 1976), while no significant effects can be ascribed to Fe^{2+}_{M1}. The relationships between the volume of *M*1, V_{M1} and $Al^{VI} \rightleftharpoons Mg^{2+}$ substitution is illustrated in Fig. 2. The V_{M1} decrease is related to the shortening of all the $<M1-O>$ bond distances.

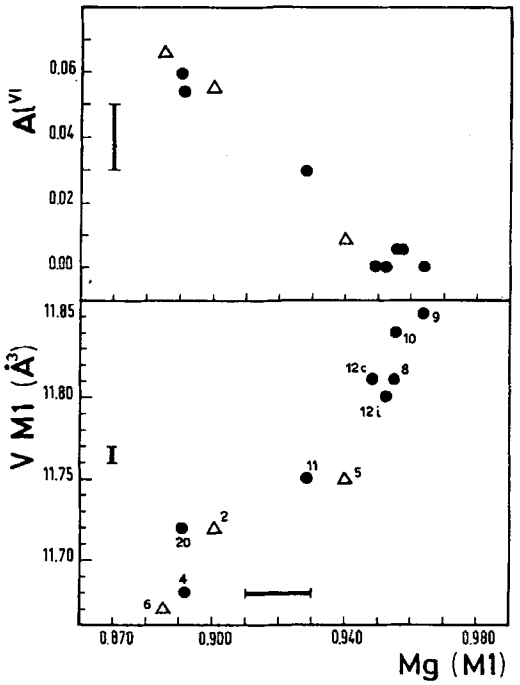

FIG. 2. Relationships between occupancy of *M*1 by Mg with volume of *M*1 site (V*M*1) and occupancy of *M*1 by Al^{VI}, respectively. Symbols as in Fig. 1. Analytical error indicated by bar.

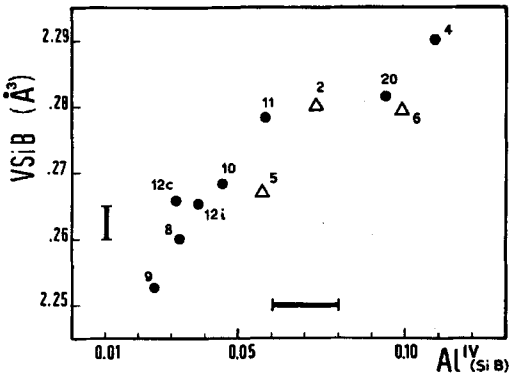

FIG. 3. Relationship between occupancy of *TB* site by Al^{IV} and volume of *TB* site (V*TB*). Symbols as in Fig. 1.

The crystals with least Al^{VI} (LE8, LE9, LE10, LE12i, LE12c) are characterized by an *M*1 configuration close to that of synthetic enstatite (V_{M1} = 11.81 Å; $<M1-O>$ = 2.078 Å) (Ganguly and Ghose, 1979).

The variance of octahedral angles (OAV) $\sigma^2_{M1,M2}$ (Robinson *et al.*, 1971) increases slightly with R^{3+} (Tables 1, 2), like that of the *M*1 site of the coexisting clinopyroxene (Dal Negro *et al.*, 1984).

The *TB* tetrahedron is the only one in which $Si-Al^{VI}$ substitution takes place. This is closely related to the $Mg^{2+}-R^{3+}$ occupancy in the *M*1 site, due to charge balance requirements. As Al^{IV} (larger than Si^{4+}) occupies *TB*, the $<TB-O>$ distances are extended and the *TB* volume V_{TB} increases (Fig. 3). No relationship between *TB* occupancy and its tetrahedral angle variance (TAV) σ^2_{TB}, (Robinson *et al.*, 1971) is observed, while the *TA* shows an increase in its TAV, σ^2_{TA}, as the orthopyroxene becomes poorer in R^{3+} (Table 2). Geometrical variations in the *TA* site are very small and accounted for in terms of the *M*1 configuration (Domeneghetti *et al.*, 1985).

One of the most important parameters of the T-chain variations is the O3–O3–O3 angle (kinking angle; Papike *et al.*, 1973). The O3B–O3B–O3B angle is lower than the O3A–O3A–O3A angle (Table 2) due to the larger size of *TB*. As Si^{4+} substitutes for Al^{IV}, the O3B–O3B–O3B angle tends to increase (Fig. 4). The decrease in the O3A–O3A–O3A angle is explained in terms of the position of oxygen O2A, strictly controlled by the shortening of the $<M2-O2A>$ bond length (Table 2) which in

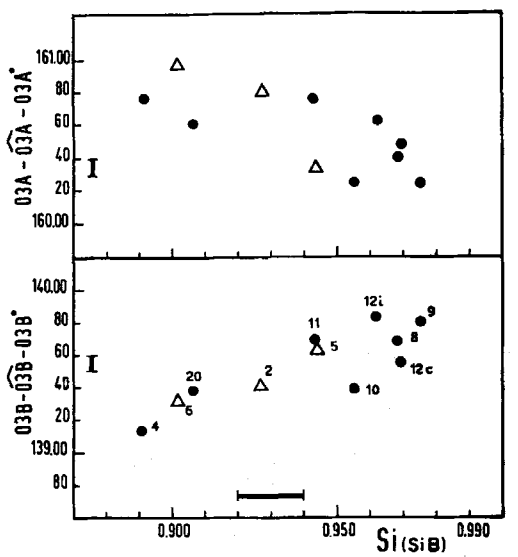

FIG. 4. Relationships between occupancy of *TB* site by Si and kink angles of *B* and *A* tetrahedral chains, respectively. Symbols as in Figs. 1 and 2.

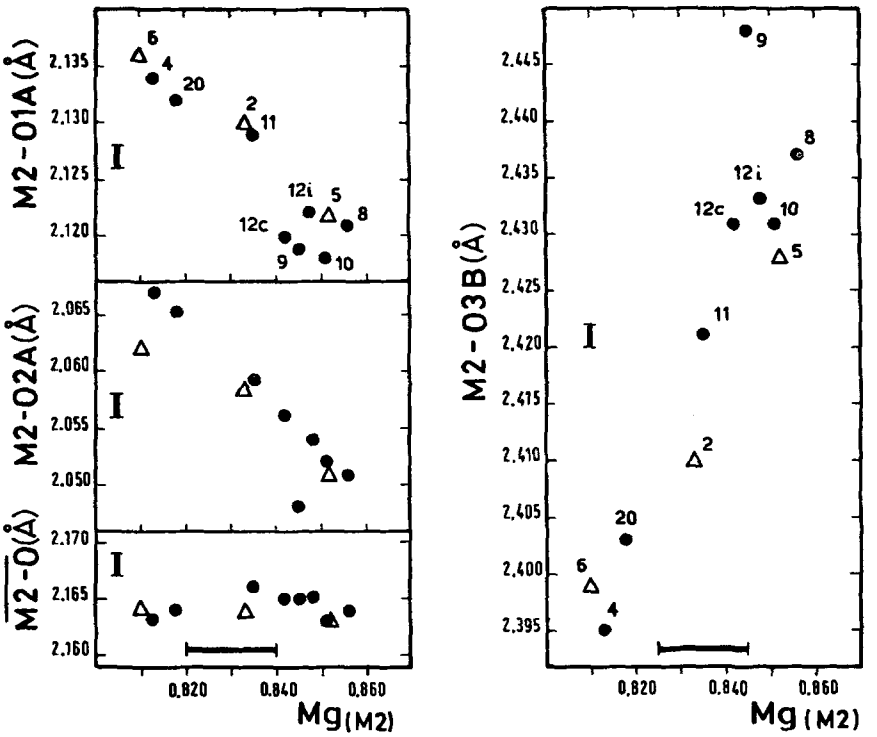

FIG. 5. Relationships between occupancy of $M2$ site by Mg and $<M2-O>$, $<M2-O2A>$, $<M2-O3B>$ bond lengths. Symbols as in Figs. 1 and 2.

turn depends on the substitution of Fe^{2+}_{M2} by Mg^{2+}_{M2}. The latter is the main occupant of $M2$ (Mg_{M2} = 0.81–0.86 atoms p.f.u.) with minor amounts of Fe^{2+} (Fe^{2+}_{M2} = 0.12–0.16 atoms p.f.u.) and Ca^{2+} (0.01–0.03 atoms p.f.u.). The $Fe^{2+}_{M2} \rightleftharpoons Mg^{2+}_{M2}$ substitution is the most important variation, constrained by $(Fe^{2+} + Ca^{2+})_{M2} > 0.14$ atoms p.f.u. The OAV variations, σ^2_{M2}, corresponding to the $Fe^{2+}_{M2} \rightleftharpoons Mg^{2+}_{M2}$ substitution, are also particularly large for virtually constant $<M2-O>$ mean bond lengths (2.163–2.165 Å) and small volume variations (12.59–12.64 Å^3). Figure 5 shows that the variation of the mean $<M2-O>$ bond length with Mg^{2+}_{M2} depends mainly on the complementary trends of $<M2-O1A>$, $<M2-O2A>$ and $<M2-O3B>$ bond lengths. Al^{IV} strongly controls the O3B position and consequently the $<M2-O3B>$ bond length (Fig. 6) (Domeneghetti *et al.*, 1985).

The highest volumes of $M2$ (V_{M2}) are generally found in crystals with the lowest contents of large cations (i.e. Fe^{2+} and Ca^{2+}). This is surprising and depends mainly on the TB–$M2$ relationship (Fig. 6). Increasing V_{M2} with loss of Fe depends

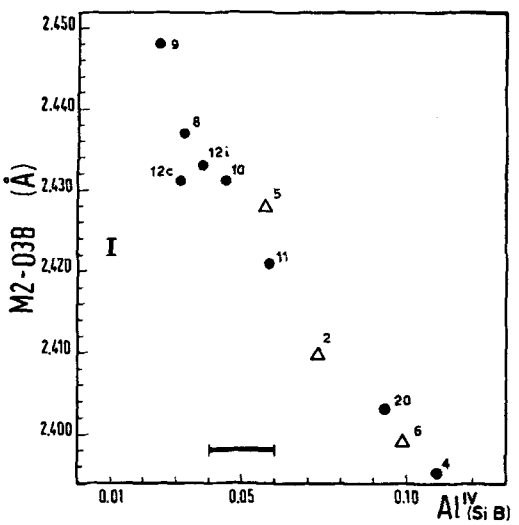

FIG. 6. Relationship between occupancy of TB site by Al^{IV} and $<M2-O3B>$ bond length. Symbols as in Figs. 1 and 2.

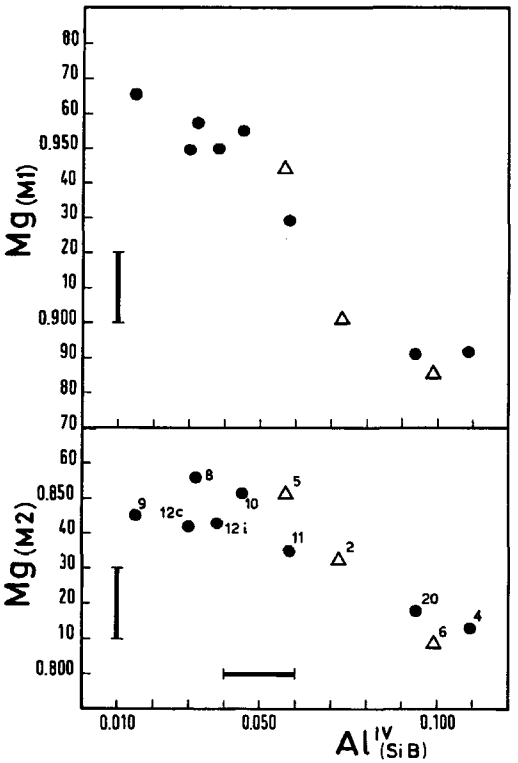

FIG. 7. Relationships between occupancy of *TB* site by Al^{IV} and occupancies of *M*2 and *M*1 sites by Mg, respectively. Symbols as in Fig. 1.

on the configuration of other polyhedra and, particularly, on the concurring contraction of V_{TB} due to loss of Al^{IV}, which varies so as to maintain (V_{M2} + V_{TB}) essentially constant. Notably, the behaviour of Fe^{2+}_{M2} in the coexisting clinopyroxene is distinct in that virtually all Fe^{2+}_{M2} is lost with increasing mg (Dal Negro *et al.*, 1984). Consequently, Fe^{2+}_{M2} is more stably retained in orthopyroxene, even in relatively Fe-poor compositions.

With increasing $(Al^{IV} \rightleftharpoons Si)_{TB}$ substitution, the increment of Mg in *M*1 is about double that for Mg_{M2} (Fig. 7). The double substitution $Al^{IV}\,Al^{VI} \rightleftharpoons Si_{TB}Mg_{M1}$ corresponds to an increase in V_{M1} (0.18 Å^3 = 15%) and V_{M2} (0.05 Å^3 = 0.4%) and a decrease in V_{TB} (0.035 Å^3 = 1.5%) and V_{TA} (0.009 Å^3 = 0.4%). These variations are distinct and significant. The variation of V_{M1} is more than three times that of V_{M2} while the latter is similar but opposite in sign to that of V_{TB}. Consequently, the variation of V_{M1} largely controls variations in cell volume, *a* and particularly *b* showing strong dependence on the octahedral cations, while *c* is less sensitive (Brown, 1967).

Discussion and concluding remarks

The degree of intra- and intercrystalline homogeneity among orthopyroxenes from the same xenolith is very high, as indicated by LE12i and LE12c. This encourages us to believe that equilibrium relationships are likely to apply to inter- and intracrystalline cation exchanges, at least within the hand specimen domain.

The crystal chemical characteristics of the investigated orthopyroxenes are mainly due to the substitution (Fig. 1)

$$(Fe^{2+}\ Al^{VI})\ Al^{IV} \rightleftharpoons Mg^{2+}\ Si^{4+} \qquad (1)$$

This substitution is related to an increase in V_{M1} (and minor V_{M2}) and a decrease in V_{TB} (and minor V_{TA}). The combined effect of (Al^{VI} + Fe^{2+}_{M1}) depletion, according to the ratio 4:1 (Fig. 1) is related to an increase in V_{M1}, mainly due to the substitution $Al^{VI} \rightleftharpoons Mg^{2+}_{M1}$. A complementary increase in Mg^{2+}_{M1} and Cr^{3+} according to the ratio 6:1 is indicated, correlated with the occupancy of *TB* by Si^{4+} and *M*2 by Mg^{2+}. The interplay of the various cations is largely dependent on Al^{IV} and Al^{VI}, due to their crystallographic effects on the *TB* and *M*1 polyhedra, respectively. The Cr^{3+} behaves as a 'refractory' element relative to Al^{VI}, as in the coexistent clinopyroxenes (Dal Negro *et al.*, 1984).

V_{M1} variations, related to the large $Al^{VI} \rightleftharpoons Mg^{2+}_{M1}$ substitution (Fig. 2) compared to the less important V_{TB} and V_{M2} variations, highlights *M*1 as the most important site in unit cell modifications (Fig. 7). The Fe^{2+} depletion occurs in both *M*1 and *M*2.

However, as Fe^{2+}_{M1} is very low (often undetected), the orthopyroxene shows a considerable amount of Fe^{2+}_{M2} (about 0.120 atoms p.f.u.) to the highest mg values (Fig. 1). This is distinct from the Fe^{2+}_{M2} depletion in the coexisting clinopyroxene, and is interpreted as a 'structural necessity' of the orthopyroxene to preserve a relatively high Fe^{2+}_{M2} content up to melting point. An explanation of this is found in the configuration of *M*2, which tends to increase in volume with decreasing $(Fe^{2+} + Ca^{2+})_{M2}$. Consequently, *M*2 favours the retention of these large cations, causing non-ideality of this Fe-depleted orthopyroxene solid solution (Virgo and Hafner, 1970; Saxena and Ghose, 1971).

According to high-temperature experiments on LE4 and LE9 orthopyroxenes (Molin, 1989), disordering of R^{3+} between *M*1 and *M*2 is not supported.

Lastly, the above orthopyroxene must be considered an ultimate Fe^{2+} carrier during partial mantle melting.

Acknowledgements

The authors are grateful to A. Cundari and E. M. Piccirillo for their critical views and suggestions. A. Cundari revised the manuscript. Financial support was provided by the Ministero dell'Università e della Ricerca Scientifica e Tecnologica and C.N.R. (Centro di Studio per la Geodinamica Alpina, Padova).

References

Brown, G. M. (1967) Mineralogy of basaltic rocks. In *Mineralogy of Basaltic Rocks. I. Basalt*, H. H. Hess and A. Poldevaart, eds., Interscience, New York. pp. 103–62.

Cundari, A., Dal Negro, A., Piccirillo, E. M., Della Giusta, A. and Secco, L. (1986) Intracrystalline relationships in olivine, orthopyroxene, clinopyroxene and spinel from a suite of spinel lherzolite xenoliths from Mt Noorat, Victoria, Australia. Comparison with related suites. *Contrib. Mineral. Petrol.*, **94**, 525–32.

Dal Negro, A., Carbonin, S., Molin, G. M., Cundari, A. and Piccirillo, E. M. (1982) Intracrystalline cation distribution in natural clinopyroxenes of tholeiitic, transitional, and alkaline basaltic rocks. In *Advances in Physical Geochemistry*, Saxena, S. K., ed., Springer Verlag, Berlin, Heidelberg, New York, **2**, 117–50.

Dal Negro, A., Carbonin, S., Domeneghetti, C., Molin, G. M., Cundari, A. and Piccirillo, E. M. (1984) Crystal chemistry and evolution of the clinopyroxene in a suite of high pressure ultramafic nodules from the Newer Volcanics of Victoria, Australia. *Contrib. Mineral. Petrol.*, **86**, 221–9.

Domeneghetti, M. C., Molin, G. M. and Tazzoli, V. (1985) Crystal-chemical implications of the Mg^{2+}–Fe^{2+} distribution in orthopyroxenes. *Amer. Mineral.*, **70**, 987–95.

Ellis, D. J. (1976) High pressure cognate inclusions in the Newer Volcanics of Victoria. *Contrib. Mineral. Petrol.*, **58**, 149–80.

Frey, F. A. and Green, D. H. (1974) The mineralogy, geochemistry and origin of lherzolite inclusions in Victorian basanites. *Geochim. Cosmochim. Acta*, **38**, 1023–59.

Ganguly, J. and Ghose, S. (1979) Aluminous orthopyroxene: order-disorder, thermodynamic properties and petrologic implications. *Contrib. Mineral. Petrol.*, **69**, 375–85

Irving, A. J. (1974) Pyroxene-rich ultramafic xenolith in the Newer basalts of Victoria, Australia. *Neues Jahrb. Mineral., Abh.*, **120**, 147–67.

James, F. and Ross, M. (1975) MINUIT, a system for function minimisation and analysis of the parameter errors and correlations. *Computer Physics*, **10** 343–7, CERN/DD, International Report **75/20**.

Molin, G. M. (1989) Crystal chemical study of cation disordering in Al-rich and Al-poor orthopyroxenes from spinel lherzolite xenoliths. *Amer. Mineral.*, **74**, 593–8.

O'Reilly, S. Y., Nicholls I. A. and Griffin, W. L. (1989) Xenoliths and megacrysts of mantle origin. In *Intraplate Volcanism in Eastern Australia and New Zealand* (Johnson, R. W., ed.), Cambridge University Press, 254–74.

Papike, J. J., Prewitt, C. T., Sueno, S. and Cameron, M. (1973) Pyroxenes: comparision of real and ideal structural topologies. *Zeits. Krist.*, **138**, 254–73.

Robinson, K., Gibbs, G. V. and Ribbe, P. H. (1971) Quadratic elongation: a quantitative measure of distortion in coordination polyhedra. *Science*, **172**, 567–70.

Saxena, S. K. and Ghose, S. (1971) Mg^{2+}–Fe^{2+} order–disorder and the thermodynamics of the orthopyroxene-crystalline solution. *Amer. Mineral.*, **56**, 532–59.

Shannon, R. D. (1976) Revised effective ionic radii and systematic studies of interatomic distances in halides and chalcogenides. *Acta Cryst.* **A32**, 751–67.

Virgo, D. and Hafner, S. S. (1970) Fe^{2+}, Mg order–disorder in heated orthopyroxenes. *Amer. Mineral.*, **55**, 201–23.

[*Manuscript received 15 March 1993: revised 13 September 1993*]